ON USING QA/QC TECHNIQUES FOR LIDAR-IMU BORESIGHT MISALIGNMENT

A. Pothou[a,*], C. Toth[c], S. Karamitsos[b], A. Georgopoulos[a]

[a] Laboratory of Photogrammetry - (apothou, drag)@central.ntua.gr
[b] Laboratory of Higher Geodesy - karamits@central.ntua.gr
School of Rural & Surveying Engineering, National Technical University of Athens, Greece

[c] Center for Mapping – toth@cfm.ohio-state.edu
The Ohio State University, Columbus, USA

The 5th International Symposium on Mobile Mapping Technology (MMT'07)

KEY WORDS: Boresight misalignment, GPS, IMU, Direct Georeferencing, MMS, LiDAR, QA/QC

ABSTRACT:

LiDAR is an effective technology for obtaining detailed and accurate terrain models from airborne platforms. High-performance integrated GPS/IMU systems provide the navigation data for the LiDAR data acquisition platform, therefore, the proper calibration of this Mobile Mapping System (MMS) is a must to determine the accurate spatial relationship of the involved sensors. This work investigates the determination of the misalignment between the IMU body frame and the LiDAR frame which is called boresight misalignment. The misalignment is determined by an adjustment during an evaluation of using a QA/QC technique (Quality Assurance/Quality Control). The processing scheme of the algorithm is based on the least squares estimation principles, and includes testing the validity, accuracy, and precision of different statistical tests for outlier detection in positioning and attitude data. In this paper, the theoretical model, results based on simulated data and a performance analysis obtained from the implementation of the algorithm, are presented. The prototype system is implemented in a Matlab environment.

1. INTRODUCTION

LiDAR (Light Detection And Ranging, also known as Airborne Laser Scanning – ALS) is a highly automated technology, with excellent vertical accuracy of point measurements, and is still improving. Although LiDAR has many benefits, and is also becoming the prime technology for large-scale acquisition of elevation data due to its capability to directly measure 3D coordinates of a huge number of points, some restrictions with regards to calibration should be strictly taken into account. LiDAR systems are complex multi-sensory systems and include at least three main sensors, GPS (Global Positioning System), and IMU (Inertial Measurement Unit, also known as INS Inertial Navigation System) navigation sensors, and the Laser-scanning device. LiDAR is assumed as a basic component of airborne Mobile Mapping Systems.

The concept of Mobile Mapping System (MMS) dates back to the late 1980s, when the Ohio State University Center for Mapping initiated the GPSVan^{TM} project, leading to the development of the first directly georeferenced and fully digital land-based mapping system in 1991 (Bossler and Toth, 1995), and the University of Calgary started a joint project with GEOFIT Inc., aimed at the development of the VISAT system designed for mobile highway mapping (Schwarz et al., 1993, El-Sheimy et al., 1995). Following the proliferation of GPS/IMU integrated technology in the mid 1990s, the quality of the Direct Platform Orientation (DPO) reached the level needed to support the demanding requirements of airborne mapping. A variety of highly specialized systems based on modern imaging sensors, such as CCD cameras, LiDAR, and hyper/multi-spectral scanners, have been developed in the last decade (Grejner-Brzezinska et al., 2002).

The factors affecting laser-target position accuracy are numerous (Schenk, 2001). Apart from the target reflectivity properties and laser beam incidence angle, the main limiting factors are the accuracy of the platform position and orientation derived from the carrier-phase differential GPS/IMU data and uncompensated effects in system calibration. The overall system calibration is a very complex task and includes individual sensor calibration, as well as the determination of the sensors' spatial relationships. High-performance integrated GPS/IMU systems provide the navigation data for LiDAR data acquisition platforms, and thus, the quality of the navigation solution is the primary factor to define the lower accuracy bound of the LiDAR point cloud. To achieve or approach the performance level of the navigation, however, the spatial relationship between the navigation sensor and the laser scanner, called the mounting bias (or offset) and the boresight, must be known with high accuracy (Toth, 2002). In most installations, the lever arms between LiDAR/GPS/IMU sensors can be determined separately by independent means, at good accuracy. In sharp contrast, the determination of the boresight angles is only possible in-flight once the GPS/IMU derived orientation becomes sufficiently accurate (Skaloud and Lichti, 2006). The misalignment between the IMU system and the scanner is the largest source of systematic error in a LiDAR and must be addressed before the sensor can be effectively deployed (Burman, 2000). In summary, the boresight misalignment is a systematic error and so should be detected and eliminated.

While several well-developed approaches for boresight estimation of Camera-IMU installations exist (see for example: El-Sheimy et al., 1995, Toth and Grejner-Brzezinska, 1998, Grejner-Brzezinska, 1999, Scaloud, 1999, Cramer et al., 2000, Kruck, 2001, Skaloud and Schaer, 2003), the correct recovery of the LiDAR-IMU misalignment still remains somewhat

* Corresponding author

elusive. Nowadays, boresight estimation between LiDAR and IMU is still heavily researched. Baltsavias, (1999) presents an overview of basic relations and error formulas concerning airborne laser scanning. Also a large number of publications report the existence of systematic errors (Schenk, 2001, Filin, 2001). The solution for dealing with and eliminating the effect of systematic errors can be categorized into two groups. One approach is based on the introduction of a correction transformation of the laser points to minimize the difference between the corresponding LiDAR points and ground truth; for instance, Kilian et. al., (1996) uses surface patches while Csanyi and Toth (2007) propose LiDAR-specific ground targets. The other technique attempts to rigorously model the system to recover the systematic errors (Burman, 2000) and treats the discrepancies between overlapping strips as orientation errors, including navigation and sensor calibration errors. Since the ground surfaces are not always known, or not at the required accuracy level, preference has been given to techniques which do not require a priori knowledge of the surface. An alternative solution, proposed by Toth and Csanyi, (2001), and by Toth, (2002), independent from ground control, can determine the boresight misalignment angles using overlapping LiDAR strips, flown in different directions, collected over an unknown surface (ground truth information can also be incorporated, if available). More specifically, it was based on the observed differences between the overlapping LiDAR strips and the required precise navigation data. More recently, Friess, (2006) reported a rigorous method which is also based on block adjustment principles with the goal to geometrically correct laser point cloud. Skaloud and Lichti, (2006) modelled the systematic effects in the direct georeferencing equation and used planar features to recover the calibration parameters in a combined rigorous adjustment model.

Earlier methods, related to LiDAR strip adjustment, also approached the effects of systematic errors in the registration between overlapping point clouds (Vosselman and Maas, 2001, Filin and Vosselman, 2004). Various investigations on registration (it is also assumed as DEM matching) have been presented (Ebner and Mueller, 1986, Ebner and Strunz, 1988). Schenk et al., (2000) referred to two mathematical methods related to the registration of LiDAR data to surfaces derived by photogrammetric means. One, minimizing the distance (min D) between a point of one surface and a surface patch of the other surface (Habib and Schenk, 1999), and the second, minimizing the remaining difference along the Z-axis (min Z) (Postolov et al., 1999). Burman, 2000, and Maas, 2000, worked on the integration of point clouds by adjustment. Surface patch matching has been performed as a straight extension of least squares matching (LS3D) by Gruen and Akca, (2004). An extended literature review about co-registration between two point datasets can be found in Pothou et al. 2006a.

Currently the most common method of calibrating a LiDAR sensor is also the least rigorous: profiles of overlapping strips are compared and an experienced operator manually adjusts the misalignment angles until the strips appear to visually fit. Although practical, this approach is time consuming and labor intensive and the results do not immediately provide any statistical measure on the quality of the calibration (Morin and El-Sheimy, 2002). Furthermore, the existing methods often cannot reliably recover all three of the angular mounting parameters. The undetermined parameter(s) propagate into the subsequently captured data, therefore compromising its accuracy and any derived product. Thus, much research effort is still devoted to improve these processes. The adopted approaches are usually based on either physical boundaries or cross-sections (Schenk, 2001) or DTM/DSM gradients (Burman, 2000).

In this paper not only a new algorithm is proposed for the same objective, but also an extensive analysis of the statistical tests for QA/QC (Quality Assurance/Quality Control) will be provided. A prototype algorithm already presented (in Pothou et al., 2006b, called 'Algorithm B') as a registration algorithm between two surfaces (point datasets) is used here for observing, and subsequently determining, the boresight misalignment of LiDAR–IMU. This algorithm takes place minimizing the distances between points of one surface and surface patches of the other surface, along to the corresponding surface normals. The originality of this algorithm is mainly based on the inclusion of the transformation parameters, in the iterative least square procedure.

In Section 2, a short review of the status of multi-sensor calibration and boresight misalignment of LiDAR-IMU is provided. In Section 3, the choice of the suitable shape and the construction of a simulated dataset, which is used in this research, is described. Section 4 outlines the proposed implementation of the algorithm for the boresight misalignment, and the underlying mathematical model. In Section 5, the QA/QC techniques supported by LiDAR–IMU boresight misalignment calculation are presented. The experimental results, as well as their statistical analysis and their effects on LiDAR points, are described in Section 6. Section 7 concludes the research with suggestions for future work.

2. MULTI SENSOR CALIBRATION - BORESIGHT MISALIGNMENT

The IMU frame is usually considered as the local reference system of the MMS system, and thus, the navigation solution is computed within this frame. The spatial relationship between the laser scanner and the IMU is defined by the offset and rotation between the two systems. The critical component here is the rotation since the object distance amplifies the effect of an angular inaccuracy, while the effect of an inaccuracy in the offset does not depend on the flying height. The description of the effects of the different boresight misalignment angles is omitted here; for details see (Baltsavias, 1999). In Figure 1, the components which are included in a LiDAR system are highlighted.

To obtain the local object coordinates of a LiDAR point, the laser range vector has to be reduced to the IMU system by applying the offset and rotation between the two systems, which provides the coordinates of the LiDAR point in the IMU system. The GPS/IMU based navigation provides the orientation of the IMU frame, including position and attitude, and thus, the mapping frame coordinates can be subsequently derived. In our discussion, the determination of the boresight offset and the boresight matrix between the IMU and the laser frame is addressed, provided that sufficient ground control is available. The boresight rotation can be described by three rotation angles, ω rotation around the x-axis, φ rotation around the y-axis, and κ around the z-axis in the laser sensor frame. A discrepancy in their values results in a misfit between the LiDAR points and the ground surface, and the calculated coordinates of the LiDAR points are not correct (Toth, 2002).

Ideally, the calibration parameters should stay constant for subsequent missions.

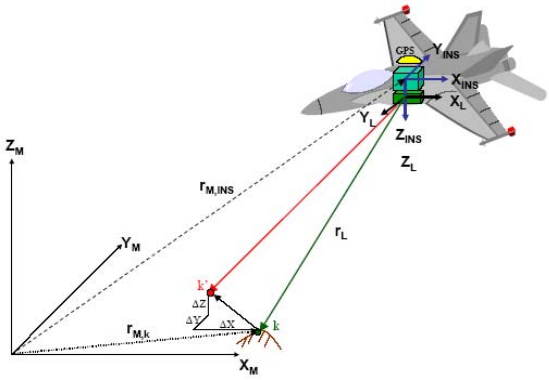

Figure 1. LiDAR System Components

Individual sensor calibrations, as well as sensor inter-calibration, are crucial for accurate and reliable operations of any MMS, especially when the highest accuracy is required. The multi-sensor calibration includes GPS/IMU lever arm (usually obtained from precision surveying, but can also be corrected during the positioning adjustment), and boresight calibration between IMU and the LiDAR sensor. Boresight calibration is referred to boresight offset (also obtained from precision surveying, usually) and boresight angle misalignment. In this project, the boresight offset is assumed as an unknown value and is included in the adjustment as three (3) more parameters, but it has to be mentioned that in case of being accurately measured it could be included in the adjustment as a constraint.

3. SIMULATION DATA

The objective of this simulation was to experimentally validate the theoretical basis of the QA/QC techniques for the boresight parameters using an ideal geometrical object. Shown in Figure 2, a "truncated" pyramid lying on a box (the base which includes 4 vertical faces) is chosen as a symmetrical shape/object in order to develop a simulated dataset similar to man-made structures, such as buildings. The size of the pyramid is: 10m x 10m base, 5m x 5m top, 5m height, and the height of the box is 5m. The whole symmetrical shape of the object and the dimensions were chosen to be similar to that of a building. By linearly interpolating this object's skeleton, a regularly-spaced TINs model was created with a point spacing of 20cm. This was used as the control point dataset, symbolized as $P=\{p_1, p_2,\ldots, p_n\}$. In Pothou et.al., 2006b, one can find the descriptions of the processing steps which are performed to the control dataset to overcome the 2D Delaunay's triangulation limitations and to produce a dense TINs model. In addition, an irregularly-spaced simulated LiDAR point cloud, with density of 5-10 points/m^2 was created, referenced as $Q=\{q_1, q_2,\ldots, q_m\}$.

In subsequent processing, the boresight misalignment values were assumed to be comparable to the LiDAR sensor's and IMU device's uncertainties. The actual values were equal to 20cm of offset (b_x=20cm, b_y=-20cm and b_z=20cm), and 5'' of rotation (ω=5'', φ=-5'' and κ=5''). Therefore, this offset and rotation were applied to the observations simulating the LiDAR points. Also, different levels of noise have been added to the observed LiDAR points for testing the algorithm, and different uncertainty values of outliers were added at the end to check the algorithm's ability for accurate detecting and eliminating blunders.

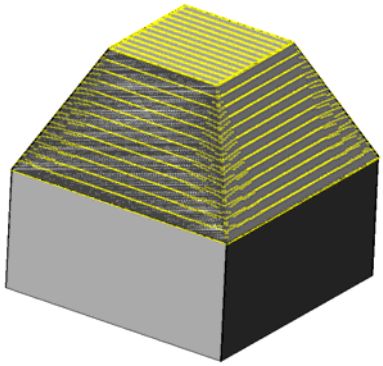

Figure 2. Simulated datasets (no noise and outliers added)

4. IMPLEMENTATION OF THE ALGORITHM

The surface on which the local surface patches (TINs) were created is referred to as the control surface (usually derived by photogrammetric means). In this investigation, a 6-parameter 3D transformation is used including translations and rotations (b_x, b_y, b_z, ω, φ, κ). The scale was assumed to be equal to c=1. In our method, the distances between points of one surface (LiDAR point cloud) and surface patches of the other surface (TINs) are being minimized along the corresponding surface normals. One advantage is that the technique requires no interpolation of the LiDAR points, which would limit the pointing accuracy and, hence, the calibration accuracy. The P surface was chosen as the control reference system while the Q surface, generated by the LiDAR, was registered allowing the surfaces to be transformed to a common coordinate system as shown in Figure 3. A short presentation of the algorithm is presented in this section; the details are discussed in Pothou et al. 2006b.

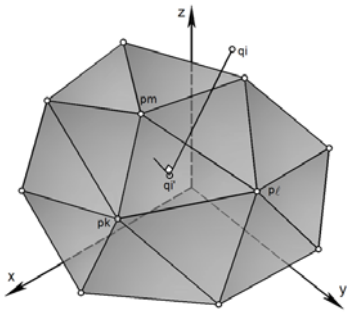

Figure 3. Point qi is a point of surface Q that is transformed to surface patch of P surface as qi´. The shortest distance from qi to the surface is used for determining the 3D transformation

Mathematical Model of the Algorithm: Assuming both the datasets as point clouds P (x_{pi}, y_{pi}, z_{pi}) (p_i= 1,…, n) and Q (x_{qi}, y_{qi}, z_{qi}) (q_i= 1,…, m) are captured by different technologies, they must be transformed into a common system. As illustrated, in Figure 3, the surface patch of the control surface P can be defined by 3 points (p_m, p_k, p_ℓ), and one point of Q point cloud has to be transformed to the closest surface patch. The projection of point q_i (x_{qi}, y_{qi}, z_{qi}) to the surface patch is described as q_i' (x_{qi}', y_{qi}', z_{qi}'). A 6-parameter 3D transformation is used for minimizing the distance between a point of Q surface and a TIN surface patch of P surface. In Equation 1, points of surface Q are transformed into the system P of the control surface.

$$\begin{bmatrix} x_p \\ y_p \\ z_p \end{bmatrix} = \mathbf{R} \cdot \begin{bmatrix} x_q \\ y_q \\ z_q \end{bmatrix} + \begin{bmatrix} b_x \\ b_y \\ b_z \end{bmatrix} \quad (1)$$

$$\mathbf{R} = \begin{bmatrix} \cos\varphi\cos\kappa & \cos\omega\sin\kappa + \sin\omega\sin\varphi\cos\kappa & \sin\omega\sin\kappa - \cos\omega\sin\varphi\cos\kappa \\ -\cos\varphi\sin\kappa & \cos\omega\cos\kappa - \sin\omega\sin\varphi\sin\kappa & \sin\omega\cos\kappa + \cos\omega\sin\varphi\sin\kappa \\ \sin\varphi & -\sin\omega\cos\varphi & \cos\omega\cos\varphi \end{bmatrix} \quad (2)$$

Where **R** (ω, φ, κ) is the orthogonal rotation matrix, defined in Equation 2, b_x, b_y, b_z are the elements of the translation vector. Since the functional model is non-linear, it is solved using an iterative least squares adjustment.

To perform least squares estimation, Equation 1 must be linearized by Taylor expansion, creating Equation 3, in matrix notation. Using the stochastic Gauss Markov model, related to a linear combination of the parameters, the observations are assumed as non-correlated. The solution of Equation 3 is developed by Equation 4, where **W** is the diagonal weight matrix of the observations. The best estimation of the vector $\hat{\mathbf{x}}$ of the parameters is given by Equation 5.

$$\mathbf{A}\delta\mathbf{x} = \boldsymbol{\delta}\ell + \mathbf{v} \quad (3)$$

$$\boldsymbol{\delta}\mathbf{x} = \left(\mathbf{A}^{\mathrm{T}}\mathbf{W}\mathbf{A}\right)^{-1}\mathbf{A}^{\mathrm{T}}\mathbf{W}\boldsymbol{\delta}\ell \quad (4)$$

$$\hat{\mathbf{x}} = \mathbf{x}^{\mathrm{o}} + \boldsymbol{\delta}\mathbf{x} \quad (5)$$

Where **A** is the design matrix, which includes as many rows as the number of observation equations that are created corresponding to the number of points in Q point cloud, and as many columns as the number of parameters. Moreover, $\boldsymbol{\delta}\mathbf{x}$ is the vector of the corrections of the approximation values $\mathbf{x}^{\mathrm{o}}$ of the unknown parameter vector **x**, $\boldsymbol{\delta}\ell = \ell - \ell^{\mathrm{o}}$ is the second part of the observation equation, and **v** the residual vector. The vector $\boldsymbol{\delta}\ell$ is calculated by the subtraction of the right part from the left part of Equation 1 using the approximation values $\mathbf{x}^{\mathbf{o}}$.

The parameters of the plane's equation, which is passed from the 3 known points (p_m, p_k, p_ℓ), are given by the 4 derivatives in Equation 6.

$$A = \begin{vmatrix} y_{pm} & z_{pm} & 1 \\ y_{pk} & z_{pk} & 1 \\ y_{p\ell} & z_{p\ell} & 1 \end{vmatrix} \quad B = \begin{vmatrix} x_{pm} & z_{pm} & 1 \\ x_{pk} & z_{pk} & 1 \\ x_{p\ell} & z_{p\ell} & 1 \end{vmatrix}$$
$$\mathbf{C} = \begin{vmatrix} x_{pm} & y_{pm} & 1 \\ x_{pk} & y_{pk} & 1 \\ x_{p\ell} & y_{p\ell} & 1 \end{vmatrix} \quad D = \begin{vmatrix} x_{pm} & y_{pm} & z_{pm} \\ x_{pk} & y_{pk} & z_{pk} \\ x_{p\ell} & y_{p\ell} & z_{p\ell} \end{vmatrix} \quad (6)$$

Based on Equation 6, the coordinates of q_i' (x_{qi}', y_{qi}', z_{qi}'), projection of point q_i (x_{qi}, y_{qi}, z_{qi}) on the plane (p_m, p_k, p_ℓ), are given by Equation 7.

The initial approximation values of the unknown parameters are set equal to zero. The transformation is applied providing the coordinates of $q_{i'}$ point by the already transformed point in the P surface. As a result, the coordinates of $q_{i'}$ point are represented as a function of the 6 transformation parameters (Equation 7). In matrix notation, Equation 8 can represent the entire system, where one can easily realize that in the observation equation the plane's parameters are also included.

$$\begin{aligned} x_{qi'} &= x_{qi} - \frac{AAx_{qi}}{A^2+B^2+C^2} + \frac{BAy_{qi}}{A^2+B^2+C^2} - \frac{CAz_{qi}}{A^2+B^2+C^2} + \frac{DA}{A^2+B^2+C^2} \\ y_{qi'} &= y_{qi} + \frac{ABx_{qi}}{A^2+B^2+C^2} - \frac{BBy_{qi}}{A^2+B^2+C^2} + \frac{CBz_{qi}}{A^2+B^2+C^2} - \frac{DB}{A^2+B^2+C^2} \\ z_{qi'} &= z_{qi} - \frac{ACx_{qi}}{A^2+B^2+C^2} + \frac{BCy_{qi}}{A^2+B^2+C^2} - \frac{CCz_{qi}}{A^2+B^2+C^2} + \frac{DC}{A^2+B^2+C^2} \end{aligned} \quad (7)$$

Equation 8 is developed by importing Equation 1 to Equation 7. Where **T** represents the symmetrical transformation matrix of x, y, z, and **L** is the matrix of constant values. In order to make the distance q_i-$q_{i'}$ equal to zero, Equation 8 should satisfy Equation 1, for any q_i point, according to Equation 9. This Equation 9 is the new observation equation for any point. It must be linearized by Taylor expansion (regarding the 6 parameters: b_x, b_y, b_z, ω, φ, κ) while $\ell = \mathbf{0}$ and ℓ^{o} is the result of Equation 9 using approximation values of 6 parameters.

$$\begin{bmatrix} x_{qi'} \\ y_{qi'} \\ z_{qi'} \end{bmatrix} = \mathbf{T} \cdot \left(\mathbf{R} \cdot \begin{bmatrix} x_{qi} \\ y_{qi} \\ z_{qi} \end{bmatrix} + \begin{bmatrix} b_x \\ b_y \\ b_z \end{bmatrix} \right) + \mathbf{L} \quad (8)$$

$$\begin{aligned} &\mathbf{T} \cdot \left(\mathbf{R} \cdot \begin{bmatrix} x_{qi} \\ y_{qi} \\ z_{qi} \end{bmatrix} + \begin{bmatrix} b_x \\ b_y \\ b_z \end{bmatrix} \right) + \mathbf{L} - \mathbf{R} \cdot \begin{bmatrix} x_{qi} \\ y_{qi} \\ z_{qi} \end{bmatrix} - \begin{bmatrix} b_x \\ b_y \\ b_z \end{bmatrix} = \mathbf{0} \Leftrightarrow \\ &(\mathbf{T} - \mathbf{I}) \cdot \left(\mathbf{R} \cdot \begin{bmatrix} x_{qi} \\ y_{qi} \\ z_{qi} \end{bmatrix} + \begin{bmatrix} b_x \\ b_y \\ b_z \end{bmatrix} \right) + \mathbf{L} = \mathbf{0} \end{aligned} \quad (9)$$

The contribution of this algorithm, given by Equations 8 and 9, is that both are functions of **T** and **L** matrices. Therefore, they depend on the surface, which is approximated by the points. In this research the plane was this surface. With the same methodology corresponding equations can also be developed for different kinds of surfaces.

5. ON USING QA/QC TECHNIQUES

To assure the quality of the data (QA-Quality Assurance), independent measurements are used to check the accuracy of the solution. If the differences are significant, an iterative correction procedure can be applied to reduce the error (QC-Quality Control). In this investigation, simulated datasets were used, and therefore, the parameters' real values were always known for accurate checking of the QA. In addition, outliers were added for the statistical quality analysis.

Through the iterative adjustment algorithm, QA/QC tests are simultaneously performed to check the internal reliability of the model. Due to the huge number of observations, a significant degree of freedom (r) exists. Firstly, a χ^2 test is performed, in the whole model, checking the ratio $\frac{\hat{\sigma}_o^2}{\sigma_o^2}$ with a 99% level of confidence. If the results are acceptable, the data snooping takes place. Each observation is tested separately, checking the ratio $\frac{v}{\sigma_v}$, in the normal distribution, with a 99% level of confidence.

Sequentially, some observations should be eliminated and the adjustment is repeated.

6. EXPERIMENTS AND RESULTS

The developed method for boresight misalignment was implemented in a Matlab environment and simulated data was used to test the adjustment model and to assess its performance. Various parameter values were used in several tests. A boresight misalignment of 20cm of offset (b_x=20cm, b_y=-20cm and b_z=20cm) and 5'' of rotation (ω=5'', φ=-5'' and κ=5'') was decided as realistic, and consequently, used as offset and rotation applied to the observations simulating the uncertainties of the LiDAR points.

In the first phase, when no noise or outliers were added, the results for both offset and rotation were satisfactory. The offset and rotation were almost totally recovered in three iterations (sequentially 80%, 19% and 1% of the offset was recovered in each iteration). Therefore, it could be said that the implemented algorithm works correctly.

Different levels of noise were added at the simulation of the LiDAR points to check the model's ability. Based on Baltsavias, 1999, LiDAR's uncertainty is, in general, defined in the range of 5-20cm. Table 1 shows five different noise levels as well as the results obtained for each case.

Table 1. Standard Deviation of boresight parameters

Offset parameters' standard deviation			**Rotation parameters' standard deviation**		
σ_x	σ_y	σ_z	σ_ω	σ_φ	σ_κ
Noise σ_x=σ_y=σ_z=20cm					
2.5mm	2.5mm	2.1mm	2'	2'	1.5'
Noise σ_x=σ_y=σ_z=5cm					
0.9mm	0.9mm	0.7mm	0.5'	0.5'	0.5'
Noise σ_x=σ_y=σ_z=10cm					
1.7mm	1.7mm	1.4mm	1'	1'	0.9'
Noise σ_x=σ_y=20cm, σ_x=10cm					
3mm	3mm	2mm	2'	2'	1'
Noise σ_x=σ_y=10cm, σ_z=5cm					
1.6mm	1.5mm	1.2mm	1'	1'	0.7'

Based on these results, the following statement could be made:

- Both offset's and rotations' direction (with the sign) are detected with standard deviation of 0.9-3mm and 0.5'-2' respectively.
- The difference between the real values (the real values are known because of the simulated data here) and the recovered values of boresight parameters are in the range of 0.1-2cm and 0.5'-8', respectively.
- The lesser the noise the better the recovery of boresight parameters.

In the next experience, various uncertainty levels of outliers were added to check the proposed method's ability for accurate boresight parameter detection and elimination of blunders. Adding outliers in the amount of 2% (100 random outliers in our case) of the total LiDAR number points, the following two QA/QC tests were performed. The first dataset, shown in Figure 4, had outliers of $\sigma_{outliers}$=2m, and the second one had outliers of $\sigma_{outliers}$=5m. Note that the $\sigma_{outliers}$=5m gives a few points over 10-15m (3σ), which actually is a big variation, and similarly $\sigma_{outliers}$=2m gives a few points over to 4-5m. A priori σ_o=1, and σ=0.2m (for the observations) were assumed. The σ is changed in every test in order to make the χ^2 test acceptable.

Outliers were removed sequentially (groups of outliers); the adjustment process had to start all over again. In Figures 6 and 7, one can see that the results were getting better as more outliers were removed. In particular, after having removed 50-60% of the outliers, the offset's and rotation's standard deviation are in the range of 2-1.3mm and 2'-0.7', respectively. The offset's difference is 0-2cm and the rotation's difference is 1'-8'. This indicates that the method works even if a limited number of small outliers are present.

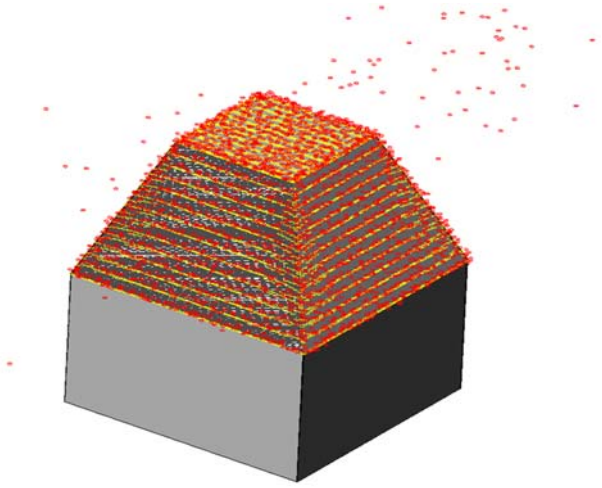

Figure 4. Pyramid with outliers of σ=2m

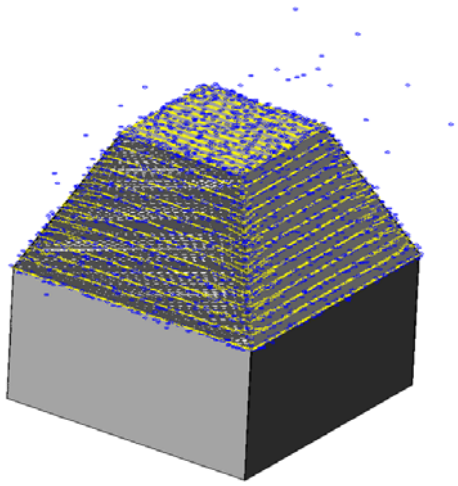

Figure 5. Having removed over 60% of outliers, sequentially

In the second case with the outliers of $\sigma_{outliers}$=5m, the results of boresight rotation are unacceptable; even the smaller number of outliers are causing problems as their value is still big (almost 5m). As far as boresight offset is concerned, however, the parameter values can be detected at 100% level. In the diagrams of Figures 6 and 7, the correlation between the standard deviations of boresight parameters and the number of removed outliers is shown. Note, the diagrams are referred to as the best case of adding noise (σ_x=σ_y=10cm, σ_z=5cm) and of adding outliers ($\sigma_{outliers}$=2m). In Figure 6, the exponential curves represent σ_x, σ_y, and σ_z in blue, green, and red, respectively. In Figure 7, the blue, green, red curves represent the σ_ω, σ_φ, σ_κ respectively. In both diagrams, the black curve shows the mean standard deviation.

7. CONCLUSIONS – FUTURE WORK

The misalignment between the IMU and LiDAR systems is the largest source of systematic errors in airborne MMS, and must be addressed before the sensor can be effectively utilized. The aim of this research is not only to develop an algorithm for boresight misalignment estimation, but also to provide an extensive analysis of the QA/QC statistical tests.

Simulated datasets were constructed for evaluating the algorithm. The proposed method was implemented, tested, and evaluated for detecting the boresight vector and the boresight attitude misalignment. Using simulated data, various LiDAR noise were used for the performance evaluation. Generally, the achievable accuracy depends on the density and the shape of TINs. In other words, it depends on how well the object can be described by the TINs.

For the QA/QC process, outliers were added and the internal reliability of the model, by χ^2 test, was checked. Moreover, the ability of the algorithm to detect and remove outliers was examined. As the big outliers are being removed from the dataset, the final parameters' results are quickly improving. Also, results are becoming smoother when all the big outliers are removed. Having removed more than 50-60% of the outliers, the convergence is quickly achieved and the results are acceptable. This indicates that the method works even if a limited number of small outliers are present. Note outliers with $\sigma_{outliers}$=2m (or less) are capable of being detected and eliminated accurately.

In the near future additional tests will be conducted using real data. Of particular interest is the introduction of a filter for detecting planar surface patches that could be used for the subsequent application of the boresight determination method. The contribution of the optimum number and positions of flat areas (as roofs), for calculating the boresight misalignment accurately will be investigated.

8. REFERENCES

Baltsavias, E.P., (1999). Airborne laser scanning: basic relations and formulas. *ISPRS Journal of Photogrammetry & Remote Sensing* 54, pp.199-214.

Bossler, J. D., and Toth, C., (1995). Accuracies Obtained by the GPSVan™, *GIS/LIS*, Vol. 1, pp. 70-77.

Burman, H., (2000). Adjustment of Laser Scanner Data for Correction of Orientation Errors. *IAPRS*, Vol. XXXIII, Part B3, pp.125-132, Amsterdam.

Burman, H., (2002). Laser strip adjustmenr for data calibration and verification. *ISPRS Journal of Photogrammetry & Remote Sensing*, Com VI, Symposium, part A, WG VI/4, Graz, Austria

Cramer, M., and Stallmann, D., (2002). System calibration for direct georeferencing. *IAPRS,* 34 (Part 3A), pp:79–84.

Csanyi, N., and Toth, C., (2007). Improvement of LiDAR Data Accuracy Using LiDAR-Specific Ground Targets, *PE&RS,* Volume 73, Number 4.

Ebner, H., and Mueller F., (1986). Processing of Digital Three Line Imagery using a generalized model for combined point determination. *IAPRS,* 26(3/1) pp.212-222.

Ebner, H., and Strunz G., (1988). Combined point determination using Digital Terrain Models as control information. *IAPRS*, 27(B11/3) pp.578-587.

El-Sheimy, N., Schwarz, K. P., Gravel, M., (1995). Mobile 3-D Positioning Using GPS/INS/Video Cameras, *Mobile Mapping Symposium, OSU Center for Mapping*, pp. 236-249.

Filin, S., (2001). Recovery of Systematic Biases in Laser Altimeters Using Natural Surfaces. *IAPRS,* Vol. XXXIV, Part 3/W4, pp. 85-91.

Filin, S., Vosselman, G., (2004). Adjustment of airborne laser altimetry strips. *IAPRS,* 34 (Part B3), pp.285–289.

Friess, P., (2006). Toward a rigorous methodology for airborne laser mapping. *International Calibration and Orientation Workshop EuroCOW* 2006, Spain.

Grejner-Brzezinska, D. A., (1999). Direct Exterior Orientation of Airborne Imagery with GPS/INS System: Performance Analysis, *Navigation*, vol. 46, No. 4, pp.261-270.

Grejner-Brzezinska, D. A., (2002). Direct Georeferencing at The Ohio State University: A Historical Perspective, *PE&RS,* Volume 68, Number 6 .

Gruen, A., and Akca D., (2004). Least Squares 3D Surface Matching. *IAPRS*, *"Panoramic Photogrammetry Workshop",* Dresden, Germany, vol. XXXIV, part 5/W16 (on CD-ROM).

Habib, A., and Schenk T., (1999). A new approach for matching surfaces from laser scanners and optical sensors. *IAPRS*, 32(3-W14) pp.55–61.

Kilian J., Haala, N., Englich, M., (1996). Capture and Evaluation of Airborne Laser Scanner Data. *IAPRS*, Vol. XXXI, Part B3, pp. 383-388, Vienna.

Kruck, E., (2001). Combined IMU Sensor Calibration and Bundle Adjustment with BINGO-F. *OEEPE Workshop "Integrated Sensor Orientation",* Hannover.

Maas, H.G., (2000). Least-Squares Matching with airborne laserscanning data in a TIN structure. *IAPRS,* 33(3A)

Morin, K., El-Sheimy, N., (2002). Post-mission adjustment of airborne laser scanning data, *Proceedings XXII FIG International Congress*, Washington DC, USA, CD ROM.

Postolov, Y., Krupnik, A., and McIntosh K., (1999). Registration of airborne laser data to surfaces generated by Photogrammetric means. *IAPRS*, 32(3/W14) pp.95-99.

Pothou A., Karamitsos S., Georgopoulos A., and Kotsis I., (2006a). Performance evaluation for aerial images and airborne Laser Altimerty dara registration procedures. *ASPRS,* Nevada.

Pothou A., Karamitsos S., Georgopoulos A., and Kotsis I., (2006b). Assessment and comparison of registration algorithms between aerial images and laser point clouds, *ISPRS*, Com. 1, *Symposium:'From sensor to imagery'* WGI/2, Part A, France.

Schwarz, K. P., Chapman, M., Cannon, M. E., and Gong, P., (1993): An Integrated INS/GPS Approach to the Georeferencing of Remotely Sensed Data, *PE&RS*, Vol. 59/11, pp. 1667-1674.

Skaloud, J., and Schaer, P., (2003). Towards a more rigorous boresight calibration, *ISPRS Workshop on Theory Technology and Realities of Inertial/GPS/Sensor Orientation*, Castelldefels, Spain, (on CDROM).

Skaloud, J., and Lichti D., (2006). Rigorous approach to boresight self-calibration in airborne laser scanning, *ISPRS, Journal of Photogrammetry & Remote Sensing* 61 pp. 47-59.

Schenk, T., Krupnik A., and Postolov Y., (2000). Registration of airborne laser data to surfaces generated by Photogrammetric means. *IAPRS*, 32(3/W14) pp.95-99.

Schenk, T., (2001). Modeling and Analyzing Systematic Errors in Airborne Laser Scanners. *Technical Notes in Photogrammetry,* vol. 19. The Ohio State University, Columbus, USA.

Toth, C., Csanyi, N., and Grejner Brzezinska, D. A., (2002). Automating the Calibration Of Airborne Multisensor Imaging Systems, *ACSM/ASPRS/FIG Congress and Annual Conference*, Washington, DC, CD ROM.

Toth, C., (2002). Calibrating Airborne LIDAR Systems, ISPRS Commission II Symposium on Integrated Systems for Spatial Data Production, Custodian and Decision Support, *IAPRS*, Vol. XXXIV, part 2, pp.475-480.

Toth, C., and Csanyi, N., (2001): Automating the LIDAR Boresight Misalignment, *ISPRS WGII/2 Workshop on Three-Dimensional Mapping from InSAR and LIDAR*, Banff, Alberta, Canada, CD ROM.

Toth, C., and Grejner-Brzezinska, D. A., (1998), Performance Analysis of the Airborne Integrated Mapping System (AIMS™), *ISPRS Comm. II Symposium 'On Data Integration: Systems and Techniques*, Cambridge, England, pp.320-326.

Vosselman, G., Maas, H.-G., (2001). Adjustment and filtering of raw laser altimetry data. *Airborne Laser scanning and Interferometric SAR for Detailed Digital Elevation Models. OEEPE Publication*, Vol. 40, pp. 62–72, Sweden.

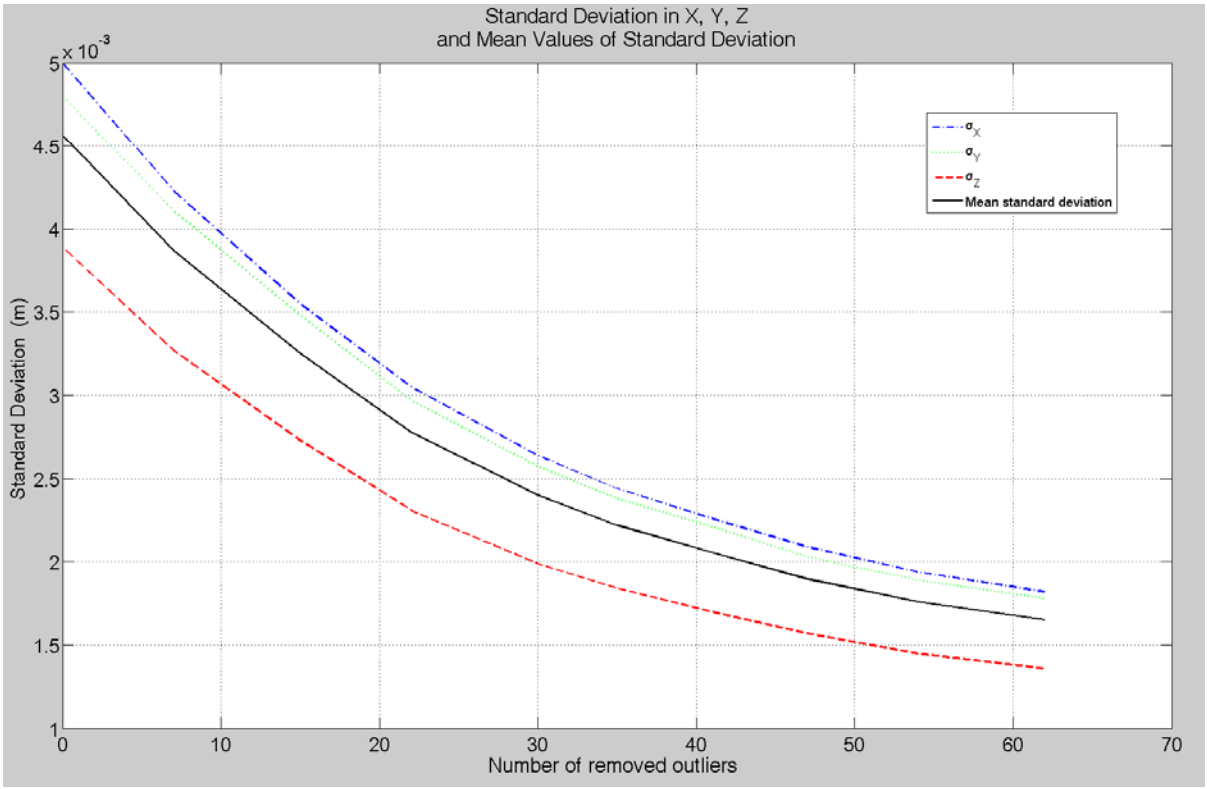

Figure 6. Standard deviation of boresight parameters (b_x, b_y, b_z) for noise $\sigma_x=\sigma_y=10$cm, $\sigma_z=5$cm (adding outliers $\sigma=2$m)

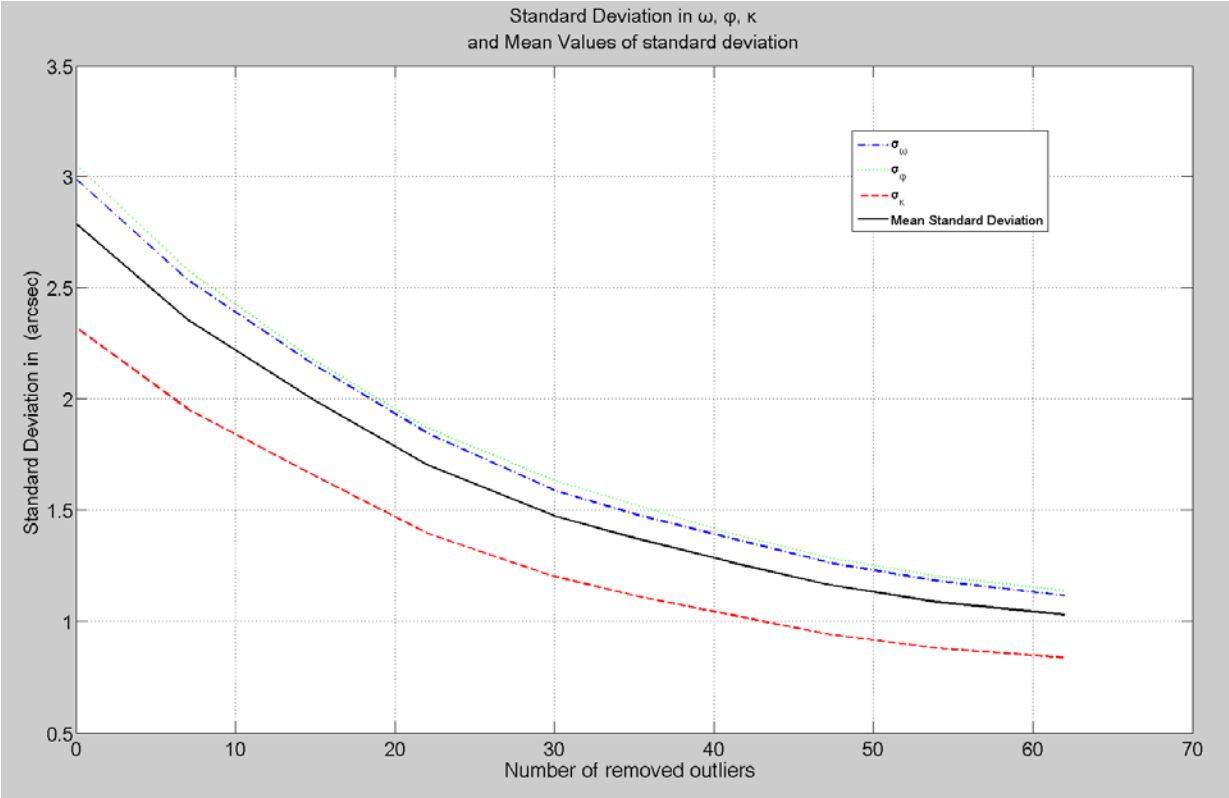

Figure 7. Standard deviation of boresight parameters (ω, φ, κ) for noise $\sigma_x=\sigma_y=10$ cm, $\sigma_z=5$cm (adding outliers $\sigma=2$m)